Sulfur Isotopic Fractionation in Vacuum Ultraviolet Photodissociation of Hydrogen Sulfide: Potential Relevance to Meteorite Analysis.

Subrata Chakraborty[a], Teresa L. Jackson[a], Musahid Ahmed[b] and Mark H. Thiemens[a]

[a]Department of Chemistry and Biochemistry, University of California, San Diego, La Jolla, California 92093-0356

[b]Chemical Sciences Division, Lawrence Berkeley National Laboratory, 1 Cyclotron Road, Berkeley, CA 94720.

Classification: Physical Sciences

Research article to PNAS as part of the Chemistry and Applications in Nature of Mass Independent Isotope Effects Special Feature

Abstract

Select meteoritic classes possess mass independent sulfur isotopic compositions in sulfide and organic phases. Photochemistry in the solar nebula has been attributed as the source of these anomalies. Hydrogen Sulfide (H_2S) is the most abundant gas phase species in the solar nebula and photodissociation of H_2S by solar vacuum ultraviolet (VUV) photons (especially by Lyman-α radiation) is potentially a relevant process. Due to experimental difficulties associated with accessing VUV, no data exists to test the hypothesis of a photochemical origin of mass independent sulfur and a theoretical basis does not exist. Here, we present multi sulfur isotopic measurements of elemental sulfur produced during the VUV photolysis of H_2S. Mass independent sulfur isotopic compositions are observed. The observed isotopic fractionation patterns are wavelength dependent. VUV photodissociation of H_2S takes place through several predissociative channels and the measured mass independent fractionation is most likely a manifestation of these processes. Meteorite sulfur data are discussed in light of the present experiments and suggestions are made to guide future experiments and models.

/body

Oxygen and sulfur are the only two elements in solar system silicates which process an isotopic abundance anomaly at the whole meteorite level (1-3). Both elements belong to Group VI and are the third and tenth most abundant elements in the solar system (with S/O ratio of 2.1 %) (4, 5), respectively. Similar to oxygen, sulfur possesses multiple stable isotopes (masses 32, 33, 34 and 36 a.m.u. with natural abundances of 95.02, 0.75, 4.21 and 0.02 %, respectively). In an oxidizing environment, oxygen condenses to high temperature (refractory) minerals, likewise, sulfur directly condenses in refractory phases under reducing conditions in the solar nebula (Figure 1) (6). Oxygen is partitioned between two major oxygen bearing molecules, e.g., CO and H_2O with fractions of 1/2 and 1/3, respectively (the rest reside in solid oxides), whereas H_2S is the major sulfur carrying gas under solar nebular conditions (4, 7). There are several other minor sulfur bearing gas phase species that exist in the solar nebula such as SiS, OCS, CS_2, CS, NS, SO, and SO_2 because of multiple available chemical valence states (S^{2-} to S^{6+}) (5, 8-10). Oxygen and sulfur are two chemically distinct entities and exist independently in the solar nebula. However, as a consequence of sulfur chemistry, it has been shown that the abundance of H_2S is severely affected by the abundance of oxygen in the solar nebula (9).

Sulfur in Chondritic Meteorites. Chondritic meteorites are one of the most primitive classes of meteorites containing round shaped mm to cm sized glassy balls (chondrules). Chondrules are one of the earliest formed solids in the solar system, composed mainly of ferromagnesian silicates with associated Fe–Ni metal and minor sulfide phases (11). Sulfur is abundant in chondrules and chondrites. The weight percent of FeS varies across a wide range, with typical abundance of 5 to 6 % and in certain mineral phases, as high as 15% (12). The heavy sulfur isotope ($\delta^{34}S$)* in sulfide phases from ordinary and enstatite chondrites (bulk analysis) are fractionated within a couple of permil from the value of Canyon Diablo Troilite (CDT) and are indistinguishable from each other (Figure 2a) (6, 13, 14). The extent of isotopic composition in carbonaceous chondrites is significantly higher (~ 14 ‰) and aqueous alteration was suggested on the chondrite parent body (14, 15) leading to formation of sulfates from sulfide grains

* Sulfur isotope ratios are written in terms of $\delta^{33}S$, $\delta^{34}S$ and $\delta^{36}S$. These "delta" values refer to the per mil difference from the ratio in a standard reservoir (j) such that $\delta^i S = (({}^iS/{}^{32}S)/({}^iS/{}^{32}S)_j - 1) \times 10^3$, where i refer to either 33, 34 or 36. For sulfur isotopes, the standard reservoir j is Canyon Diablo Troilite (CDT). $\Delta^{33}S$ and $\Delta^{36}S$ represent the degree of mass independent fractionation and are defined as $\Delta^{33}S = \delta^{33}S - 0.515\delta^{34}S$ and $\Delta^{36}S = \delta^{36}S - 1.9\delta^{34}S$. These quantities represent the departure from the mass dependent (e.g., $\Delta^{33}S$, $\Delta^{33}S = 0$) fractionation.

enriching the sulfide in heavy sulfur isotopes. It has been shown that the sulfur isotopic composition in individual chondrules and matrix material is normal (mass dependent), except for the chondrules from the Dhajala (H3) chondrite, which posses a slight mass independent component (Figure 2b, $\Delta^{33}S \sim 0.11$ ‰). The chondrule rim material has been suggested as the source of this anomaly. Apart from silicates, organic isolates (methyl (MSA), ethyl (ESA), isopropyl (iPSA), and *n*-propyl (nPSA) sulfonic acids) from Murchison (Carbonaceous Chondrite) also reveal a large mass independent sulfur composition (upto ~ 2 ‰ in $\Delta^{33}S$ and $\Delta^{36}S$) (16).

Sulfur in Achondritic Meteorites. The typical weight percent of FeS in achondrites is about 0.5, or ~ 10 times lower than that in chondrites (12). The range of heavy isotope fractionation ($\delta^{34}S$) in different types of achondrites is small compared to that of ordinary and enstatite chondrites (17). Mass independent sulfur isotopic compositions (enrichment in ^{33}S) has been reported in achondritic meteorites such as Ureilites, Oldhamite (CaS) in the Norton county, Aubrite, and Acapulcoite-Lodranites (17, 18) (Figure 2b). In another enigmatic achondrite group, Ureilites, a range of ^{33}S anomalies has been observed which extending from 0.02 to 0.1 ‰ (Figure 2b) (18, 19).

Several possible sources of mass independent sulfur measured in meteorites have been suggested (17). A photochemical origin is considered to be one of the viable mechanisms. Photochemistry plays a significant role in shaping the chemical reaction network in the solar nebula and interstellar clouds (5, 10, 20-26). Laboratory based photochemistry experiments have provided some verification that the isotopic fractionation during photolysis of various sulfur containing molecules by UV photons is mass independent (27-29). Determination of the isotope effect in the VUV photodissociation of relevant triatomic molecules such as H_2S and H_2O is of importance to fully understand the oxygen and sulfur isotopic signatures recorded in the meteorites. In this paper we report the first experiments that measure the multi sulfur isotopic fractionation during VUV photodissociation of H_2S. There is presently no experimental data at relevant VUV wavelengths to display the role of H_2S photolysis in the early solar system. A limited set of data exists for UV wavelengths (>250 nm), which show mass dependent sulfur

isotopic fractionations (28). The new experimental results at short wavelength and potential relevance to the early solar nebula are discussed.

Results and Discussion

The sulfur isotopic composition ($\delta^{33}S$, $\delta^{34}S$, and $\delta^{36}S$) of product elemental sulfur is enriched with respect to initial H_2S (except for two samples at 90 and 139.1 nm photolysis products, respectively) and are shown in a combined three isotope plot, Figure 3 (shown in Table S1 of Supporting Information, SI). Photolysis at 121.6 nm (Lyman-α line) reveals a mass independent fractionation with a maximum value of -1.5 ‰ in $\Delta^{33}S$ and a corresponding $\Delta^{36}S$ value of 4.6 ‰, giving rise to a slope value of ~ -3 (with near zero intercept) in $\Delta^{33}S$ vs $\Delta^{36}S$ plot (Figure 4). Elemental sulfur produced at 139.1 nm wavelength also shows a mass independent composition, both in ^{33}S and ^{36}S, similar to that measured for 121.6 nm (Figure 4). The two elemental sulfur samples produced at 90 and 157.6 nm are spiked (with commercial Ag_2S) due to small sample size and requirements to perform isotopic measurements (see SI for detail) are associated with somewhat larger uncertainties (1 σ = 0.3 ‰ for $\Delta^{33}S$ whereas for other data, 0.1 ‰ and circled in Figure 3 and 4) and posses mass independent sulfur isotopic compositions. For 90 nm photolysis, except for this particular (spiked) sample, the other two samples show isotopic composition close to normal for ^{33}S, whereas for ^{36}S the fractionation is higher (slightly positive $\Delta^{36}S$ values). The size of these two samples (SF_6) are more than 5 micromoles and the uncertainty (1σ) associated with $\Delta^{36}S$ is less than 0.2 ‰ for this sample size. Therefore, the measured $\Delta^{36}S$ values are higher than the uncertainty limit. For 157.6 nm photolysis, except for the spiked sample, the other elemental sulfur samples yield near to normal sulfur isotopic compositions in both in ^{33}S and ^{36}S.

VUV Photochemistry and Predissociation Dynamics of H_2S. Absorption spectra of H_2S exhibit several Rydberg series in the VUV spectral region(up to 160 nm) and converge to the ionization limit beyond 90 nm (30-34). There are several experimental and theoretical spectroscopic studies (35-41) describe the photodissociation dynamics of H_2S at the experimental VUV wavelengths (i.e., 121.6, 139.1, 157.6 nm) explored in the present study. Theoretical studies (37-39, 42) suggest that two strongly coupled excited electronic states are involved in the Rydberg levels of H_2S, an upper $B\ ^1A_2$ state that is bound and the lower $A\ ^1B_1$ dissociative state. In the photodissociation process of H_2S, the molecule is first excited to the

bound state, and subsequently through coupling (of the two states) accesses the repulsive surface and predissociates (43) in several branches (35, 41):

$H_2S + h\nu \rightarrow H + SH\ (X\ ^2\Pi)$…… (1)

$\rightarrow H + SH\ (X\ ^2\Sigma^+)$…… (2)

$\rightarrow H + H + S\ (^3P)$ …… (3)

$\rightarrow H + H + S\ (^1D)$ …… (4)

$\rightarrow H_2 + S\ (^3P)$ …..…… (5)

The major difference in predissociation dynamics at different Rydberg levels for varying photoexcitation energies is that the relative contributions from the branches differ. For example, for 121.6 nm excitation, pathways 2, 3 and 4 are important (35), whereas for 157.6 nm excitation branch 1 is dominant (36, 41) and the photodissociation yields for 121.6 and 157.6 nm differ.

Predissociation from various excited states of H_2S is known to be a sensitive function of parental rotational level (not dependent on the vibrational state) and a significant isotope selectivity in predissociation is expected (38). Accidental near resonances between vibrational levels of different electronic states can significantly enhance radiationless transfer into the final dissociative state and such resonances are responsible for the vibrational level dependent predissociation. Isotope specificity due to accidental predissociation has been observed in diatomic molecular systems, including N_2 and CO (25, 44, 45). Unlike diatomic molecules, where the potential energy surface is a function of bond length, for triatomic molecules, the added variable of bond angle further complicates the dissociation dynamics (36). Moreover, the SH photofragments (equations 1 and 2) also rapidly predissociate (35) potentially generating an additional isotope effect.

Probable origin of Mass Independent Sulfur Isotopic Composition. The mass independent isotopic fractionations during UV photodissociation have been measured and theoretically calculated for triatomic molecules such as CO_2, NO_2, N_2O, SO_2 (27, 29, 46-53). There is no common physical chemical mechanism for these anomalous processes and several molecule specific mechanisms have been proposed. Quantum mechanical basis have been proposed for the various molecules involving electronic, vibrational and rotational energy states, as the origin of mass independent fractionation (47, 48, 54). One exception is a proposal involving SO_2

photolysis via isotope selective photodissociation in a column of gas producing differential photoabsorption among different isotopologues (isotope self-shielding) (51).

For isotope self-shielding to occur, the absorption spectra should posses fine structure and the absorption lines for different isotopologues must be separated in the frequency domain (55). This is not fulfilled in the VUV photoabsorption zone for H_2S (34), consequently the likely source of the mass independent isotopic fractionation observed in the present experiments is from predissociation processes associated with the different dissociation pathways. As discussed, available predissociative processes (equations 1 through 5) are not equivalent and contribute in different proportions subsequent to photoexcitation for different wavelengths. As a result, the measured isotopic compositions of elemental sulfur vary for different photolysis wavelengths, and hence generate different mass independent fractionation trends. As an illustration, the major differences in fragmentation pathways during photodissociation at 121.6, 139.1, and 157.6 nm is that the product SH fragment at 121.6 nm populates the A $^2\Sigma^+$ state, whereas it populates the X $^2\Pi$ state at the other two wavelengths. SH fragments subsequently predissociate to yield elemental sulfur in all cases (35-37, 41). Since predissociation is quantum state specific (44), the isotope effect due to predissociation of SH fragment from these two states are different and may give rise to an additional effect that varies from one state to other.

Based on the product sulfur isotopic composition measured in the present experiments, potential nebular scenarios to explain the meteoritic observations may be suggested. If H_2S is the major gas phase species and undergoes photodissociation from solar VUV or from other stellar sources, the isotopic shift in $\delta^{34}S$ of the residual H_2S reservoir would not be significant (within a few permil) and is consistent with $\delta^{34}S$ variations observed in different meteorite groups (Figure 2a) (13). The photolysis isotope data obtained in this experiment are wavelength dependent. As H_2S photolysis in the nebula occurs through the entire VUV region, an effective isotopic fractionation can be modeled combining the wavelength specific fractionation and nebular line strengths. Only four Rydberg bands are covered in the present experiments using broadband (~2 nm) VUV photons from the synchrotron and the entire VUV region was not covered and therefore, the effective fractionation in VUV photodissociation cannot be computed. However, Lyman-α (121.6 nm) is the strongest line in t-tauri phase of the sun (Figure 5) (56). The integrated absorption cross-sections at 90, 139.1, and 157.6 nm are ~ 2, 0.88, and 0.31 times, respectively, that of at 121.6 nm (Figure 5). Though the cross-section at 90 nm is twice that of

121.6 nm, the VUV flux at 121.6 nm is about 20 times more. The combination of VUV flux and cross-section renders Lyman-α as the strongest contributor in VUV photodissociation and therefore, the fractionation obtained at Lyman-α wavelength can be used instead to interpret the meteorite data though a full model treatment is clearly needed. As shown in Figure 4 there is a range in meteorite data and that is consistent with the spread measured for 121.6 nm photolysis (along the slope ~ -3 line in $\Delta^{33}S$ vs $\Delta^{36}S$ plot).

Sulfur Isotopic Composition in Chondrites. In the early stages of nebular disk evolution, a fundamental difference in the chemistry of the two volatile species H_2O and H_2S is that H_2O condenses directly to a solid at the snow line and beyond (Figure 1), whereas H_2S chemically evolves via gas-solid reactions ($Fe_{(solid)} + H_2S_{(gas)} = FeS_{(solid)} + H_{2\ (gas)}$) to form solids (9, 57). Laboratory experiments have shown that under solar nebula conditions, sulfurization of Fe (FeS or troilite formation) proceeds in the temperature range of 500 – 690 K, well within (< 2 AU) the snow line (58). This is consistent with H_2S condensation as a sulfide form in the inner solar nebula that is subsequently incorporated into chondritic and achondritic parent bodies at a later, secondary stage. Two competitive processes may arise involving H_2S. First, gas to solid condensation of H_2S as FeS in the dense midplane of the inner solar nebula may occur within 2 AU of the proto sun (Figure 1) (9, 58), and the second process, photodissociation of H_2S in the photoactive zone of the solar nebula (17). The formation of troilite is kinetically a fast process (58) and since it was operative at the dense midplane, the effective thermo chemical sulfide formation rate dominates H_2S photolysis in that zone, which is optically opaque. In this scenario, the product troilite would not possess an isotope component resulting from H_2S photolysis.

Chondrites and chondrules contain overwhelmingly large amounts of sulfur as troilite and other sulfide minerals (12). It was recently suggested that in the early solar nebula the formation of CAIs (Calcium Aluminum Rich Inclusion), the first product of condensation, was as early as 80,000 years (59) and chondrules formed within 2 My of CAIs (60), though some evidence suggest they are contemporary (61). Therefore, chondrules may have directly captured condensed troilite with no apparent mass independently fractionated sulfur. A similar proposition was suggested by (6).

Recent oxygen isotopic measurements (62) of CAIs documented systematic variation of isotopic ratios ($\delta^{18}O$, $\Delta^{17}O$) starting at the margin of CAIs indicate that they were circulated

within the solar nebula after formation and were exposed to nebular environments of different oxygen isotopic composition. This scenario may also be applicable to chondrules, where chondrule sulfide rims are formed from different gas/dust while the chondrules were circulating within the nebula and archived the isotopic composition of different nebular environments, especially on the rims. At this time, the chondrule rims might have captured the mass independent isotopic signature produced by H_2S photolysis, as measured for Dhajala chondrule rims (6). The step wise leaching protocol followed by (6) clearly demonstrate that the $\delta^{34}S$ value shifts about 2 ‰ between the chondrule interior and the rim of Dhajala, the corresponding shift in $\Delta^{33}S$ is ~0.12 ‰. The isotopic compositional shift between the chondrule interior and the rim can be best explained though the chondrule migration mechanism after formation as described (62) and exposed to a photochemically fractionated H_2S gas.

Mass Independent Sulfur Isotopes in Achondrites. A distinction of achondrites vs. chondrities is the low abundance of sulfur in achondrites, generally a factor of ~10 (12), which may provide opportunity to observe their primitive character. Oldamite (CaS) has been identified as one of the carrier phases of mass independent sulfur (17). As modeled, at the early evolutionary time period of the solar nebula, sulfur chemistry altered with changing oxygen fugacity (9). The H_2O condensation front (snow line at ~ 3 AU) in the nebula introduces a strong zoning between the inner and outer nebula (Figure 1). As water vapor was progressively diffusing out of the inner solar nebula with a rapid rate in the first 10^5 year (63, 64) , FeS was being replaced by CaS as the dominant sulfur condensate. A time scale of ~ 10^6 years was required for this change in sequence, and in that time period, the majority of sulfur condensed as FeS (9) in the chondrule formation zone. Therefore, while CaS was forming, the proportion of photochemically processed sulfur fraction increased compared to total sulfur and became the carrier phase of mass independent sulfur, archiving the signature of nebular photochemistry.

It is not precisely defined how and where chondritic and achondritic parent bodies formed and produced the quantity of sulfur contained in the planetesimals. A suggested scenario is that the achondritic parent body underwent thermal alteration at a later time stage and lost most of the volatile sulfur during this process (65); A highly refractory phase (e.g., CaS) might however, survive this thermal episode and is found in achondritic meteorites and has a mass independent sulfur composition (e.g., Norton County Aubrite (17)). Ureilites are the most enigmatic of

achondrites and show dual signature of thermal metamorphism as well as primitive texture (19). The measured sulfur isotopic compositions ($\Delta^{33}S$) process a wide range (Figure 2b) but do not correlate with oxygen isotopic anomalies (18, 66). It is inferred that the oxygen and sulfur systems are decoupled from each other and the variation and the sulfur mass independent composition reflects the extent of thermal metamorphism in ureilite parent body (or bodies) and the survival of the reduced refractory phases. The parent body of HEDs (believed to be the Vesta asteroid) is a totally differentiated body and survival of reduced refractory sulfur phases is unlikely due to large scale homogenization and hence no mass independent sulfur isotopic composition generated by photochemistry was preserved. Further studies of minor sulfide components of achondrites would be definitive in defining this process.

Mass Independent Sulfur Isotopes in Meteorite Organics. Sulfonic acid extracts from the Murchison meteorite contain mass independent sulfur isotopic compositions (16) shown in Figure 4. These anomalies are significantly larger compared to that observed in achondrites (17). Associated with the ^{33}S enrichment in organic material are high D/H ratios, which has been interpreted as being indicative of C-H bond formation at lower temperatures (67). Recently, the synthesis of organic molecules in the solar nebula has been modeled (68). It was shown that ice grains that originate in the outer nebula in a high D/H region may experience UV photochemistry from the central star or nearby stars during long range passage within the disk, and subsequently synthesize organic molecules. Association of mass independent sulfur isotopic components (as a result of VUV photodissociation of H_2S) with hydrocarbons might have occurred in the low temperature nebular regime and became a part of the organics and ultimately incorporated in the carbonaceous chondrite parent bodies during the accretion process. The sulfur isotopic anomalies measured in different organic fractions vary (Figure 4). The methyl (MSA) group is more enriched in ^{33}S compared to the other higher order hydrocarbon compounds. As discussed, migration of the ice particles and irradiation by UV radiation may be a facet of the organic synthesis process. Available VUV light at different locations of the disk is variable, especially at the surface layer of the disk and outer region of the nebula where the disk is irradiated by solar as well as external stellar sources. The stellar light is attenuated with depth of penetration of the light inside the disk by absorption of different gaseous molecules, such as H_2 and CO. This scenario allows H_2S photolysis at different VUV wavelengths in different regions in the disk

during grain migration. The present experimental results show wavelength specific mass independent fractionation (Figure 3 and 4), thus, it is plausible that different sulfur reservoirs of unique isotopic composition existed in the nebula and the icy particles recorded one of these compositions while migrating within the nebular disk.

Conclusions

Multi sulfur isotopic compositions have been measured in elemental sulfur produced during the VUV photolysis of H_2S at four different wavelength bands at the ALS synchrotron. The measured sulfur isotopic fractionations are mass independent. Photolysis at 121.6 nm (Lyman-α line), one of the most prominent lines in the t-tauri phase of the sun, yields a slope value of -3 in four-isotope $\Delta^{33}S$ - $\Delta^{36}S$ space during VUV photodissociation of H_2S. The source of mass independent sulfur isotopic composition in H_2S photodissociation is likely through a predissociative process, introducing isotope selectivity in the resonance governed curve crossing. Plausible nebular scenario is suggested to explain the sulfur isotope data from meteorites in the light of H_2S photolysis data obtained in the present experiments.

Materials and Methods

H_2S photodissociation was carried out in four different wavelength bands (90, 121.6, 139.1, 157 nm) in the VUV region using photons from the Advanced Light Source (ALS) synchrotron at Lawrence Berkeley National Laboratory. A 60 cm long window-less reaction chamber was used for this purpose, which was attached to the beamline with a three-stage differentially pumped vacuum sectors (Figure S1 of SI) as described in (25). In these flow experiments, high purity H_2S gas was passed through the reaction chamber from a lecture bottle keeping the pressure constant for a particular experiment. For each wavelength, the pressure was varied from 100 to 240 mtorr. Before flowing H_2S inside the chamber in each experiment, a pre-cleaned cylindrical aluminum jacket was coaxially inserted into the reaction chamber. After each photolysis experiment, the jacket was carefully removed and stored. During VUV photolysis of H_2S, elemental sulfur was produced (35) and was deposited on the surface of the Al-jacket. Chemically extracted elemental sulfur from the Al-jacket (at UCSD) was subsequently treated to convert to SF_6 and measured for all four stable sulfur isotopes by Isotope Ratio Mass Spectrometry (MAT 252). Full details for the experiments, process and isotope measurement are provided in the SI.

ACKNOWLEDGEMENTS. S.C. gratefully acknowledges Ryan D. Davis for his help in performing experiments at ALS. Support from Ms. Sarah Ferrell and Dr. Amir Golan of Chemical Dynamics Beamline of ALS, and Dr. Doug Taube (Chemistry Laboratory Manager of ALS) is acknowledged. The work is funded through NASA's Origins and Cosmochemistry program. MA and the ALS are supported by the Director, Office of Energy Res., U. S. Dept. of Energy (Contract No. DE-AC02-05CH11231).

References

1. Thiemens MH (2006) History and Applications of Mass-Independent Isotope Effects. *Annual Review of Earth and Planetary Sciences* 34(1):217-262.
2. Clayton RN (2007) Isotopes: From Earth to the Solar System. *Annual Review of Earth and Planetary Sciences* 35(1):1-19.
3. Thiemens MH, Chakraborty S, & Dominguez G (2012) The Physical Chemistry of Mass Independent Isotope Effects and Their Observation in Nature. *Annual Review of Physical Chemistry* 63(1):*(in Press)*.
4. Anders E & Grevesse N (1989) Abundances of the elements: Meteoritic and solar. *Geochimica Et Cosmochimica Acta* 53(1):197-214.
5. Fegley B (1999) Chemical and Physical Processing of Presolar Materials in the Solar Nebula and the Implications for Preservation of Presolar Materials in Comets. *Space Science Reviews* 90(1):239-252.
6. Rai VK & Thiemens MH (2007) Mass independently fractionated sulfur components in chondrites. *Geochimica Et Cosmochimica Acta* 71(5):1341-1354.
7. Fegley B (2000) Kinetics of gas-Grain Reactions in the Solar Nebula. *Space Science Reviews* 92(1):177-200.
8. Mandeville CW (2010) Sulfur: A Ubiquitous and Useful Tracer in Earth and Planetary Sciences. *Elements* 6:75–80.
9. Pasek MA*, et al.* (2005) Sulfur chemistry with time-varying oxygen abundance during Solar System formation. *Icarus* 175(1):1-14.
10. Irvine WM, Schloerb FP, Crovisier J, Fegley J, B., & Mumma MJ (1999) Comets: A Link Between Interstellar and Nebular Chemistry *Comets: A Link Between Interstellar and Nebular Chemistry', in Protostars and Planets IV*, eds Mannings V, Boss AP, & Russell SS (University of Arizona Press, Tucson, AZ), Vol VI.
11. Hewins RH (1997) CHONDRULES. *Annual Review of Earth and Planetary Sciences* 25(1):61-83.
12. Jarosewich E (1990) Chemical analyses of meteorites: A compilation of stony and iron meteorite analyses. *Meteoritics* 25(4):323-337.
13. Gao X & Thiemens MH (1993) Variations of the isotopic composition of sulfur in enstatite and ordinary chondrites. *Geochimica Et Cosmochimica Acta* 57(13):3171-3176.
14. Gao X & Thiemens MH (1993) Isotopic composition and concentration of sulfur in carbonaceous chondrites. *Geochimica Et Cosmochimica Acta* 57(13):3159-3169.

15. Bullock ES, McKeegan KD, Gounelle M, Grady MM, & Russell SS (2010) Sulfur isotopic composition of Fe-Ni sulfide grains in CI and CM carbonaceous chondrites. *Meteoritics & Planetary Science* 45(5):885-898.
16. Cooper GW, Thiemens MH, Jackson TL, & Chang S (1997) Sulfur and hydrogen isotope anomalies in meteorite sulfonic acids. *Science* 277(5329):1072-1074.
17. Rai VK, Jackson TL, & Thiemens MH (2005) Photochemical mass-independent sulfur isotopes in achondritic meteorites. *Science* 309(5737):1062-1065.
18. Farquhar J, Jackson TL, & Thiemens MH (2000) A S-33 enrichment in ureilite meteorites: Evidence for a nebular sulfur component. *Geochimica Et Cosmochimica Acta* 64(10):1819-1825.
19. Goodrich CA, Jones JH, & Berkley JL (1987) Origin and evolution of the ureilite parent magmas: Multi-stage igneous activity on a large parent body. *Geochimica Et Cosmochimica Acta* 51(9):2255-2273.
20. Towe KM (1993) Photochemistry in the Primitive Solar Nebula. *Science* 261(5124):1058-1059.
21. Dalgarno A & Black JH (1976) Molecule formation in the interstellar gas. *Rep. Prog. Phys.* 39:573-612.
22. Clayton RN (2002) Solar System: Self-shielding in the solar nebula. *Nature* 415(6874):860-861.
23. Lyons JR & Young ED (2005) CO self-shielding as the origin of oxygen isotope anomalies in the early solar nebula. *Nature* 435(7040):317-320.
24. Young ED (2007) Time-dependent oxygen isotopic effects of CO self shielding across the solar protoplanetary disk. *Earth and Planetary Science Letters* 262(3-4):468-483.
25. Chakraborty S, Ahmed M, Jackson TL, & Thiemens MH (2008) Experimental test of self-shielding in vacuum ultraviolet photodissociation of CO. *Science* 321(5894):1328-1331.
26. Yung YL, Friedl RR, Pinto JP, Bayes KD, & Wen J-S (1988) Kinetic isotopic fractionation and the origin of HDO and CH3D in the solar system. *Icarus* 74(1):121-132.
27. Farquhar J, Savarino J, Airieau S, & Thiemens MH (2001) Observation of wavelength-sensitive mass-independent sulfur isotope effects during SO2 photolysis: Implications for the early atmosphere. *J. Geophys. Res.* 106(E12):32829-32839.
28. Farquhar J, Savarino J, Jackson TL, & Thiemens MH (2000) Evidence of atmospheric sulphur in the martian regolith from sulphur isotopes in meteorites. *Nature* 404(6773):50-52.
29. Masterson AL, Farquhar J, & Wing BA (2011) Sulfur mass-independent fractionation patterns in the broadband UV photolysis of sulfur dioxide: Pressure and third body effects. *Earth and Planetary Science Letters* 306(3–4):253-260.
30. Watanabe K & Jursa AS (1964) Absorption and Photoionization Cross Sections of H[sub 2]O and H[sub 2]S. *The Journal of Chemical Physics* 41(6):1650-1653.
31. Masuko H, Morioka Y, Nakamura M, Ishiguro E, & Sasanuma M (1979) Absorption spectrum of the H2S molecule in the vacuum ultraviolet region. *Canadian Journal of Physics* 57(5):745-760.
32. Price WC (1936) The Far Ultraviolet Absorption Spectra and Ionization Potentials of H[sub 2]O and H[sub 2]S. *The Journal of Chemical Physics* 4(3):147-153.

33. Gallo AR & Innes KK (1975) A 1B1 Ryberg state of the H2S molecule. *Journal of Molecular Spectroscopy* 54(3):472-474.
34. Feng R, Cooper G, & Brion CE (1999) Absolute oscillator strengths for hydrogen sulphide:: I. Photoabsorption in the valence-shell and the S 2p and 2s inner-shell regions (4–260 eV). *Chemical Physics* 244(1):127-142.
35. Schnieder L, Meier W, Welge KH, Ashfold MNR, & Western CM (1990) Photodissociation dynamics of H[sub 2]S at 121.6 nm and a determination of the potential energy function of SH(A [sup 2] Sigma [sup +]). *The Journal of Chemical Physics* 92(12):7027-7037.
36. Cook PA, Langford SR, Dixon RN, & Ashfold MNR (2001) An experimental and ab initio reinvestigation of the Lyman-alpha photodissociation of H[sub 2]S and D[sub 2]S. *The Journal of Chemical Physics* 114(4):1672-1684.
37. Ashfold MNR & Dixon RN (1982) Multiphoton ionisation spectroscopy of H2S: a reinvestigation of the 1B1-1A1 band at 139.1 nm. *Chemical Physics Letters* 93(1):5-10.
38. Ashfold MNR, Bayley JM, Dixon RN, & Prince JD (1985) Molecular Photodissociation Dynamics Revealed by Multiphoton Ionisation Spectroscopy. *Berichte der Bunsengesellschaft für physikalische Chemie* 89(3):254-261.
39. Ashfold MNR, Bayley JM, Dixon RN, & Prince JD (1985) Molecular predissociation dynamics revealed through multiphoton ionisation spectroscopy. III. New 1A2 and 1B1 rydberg states in H2S D2S. *Chemical Physics* 98(2):289-313.
40. Ibuki T*, et al.* (1985) Photoabsorption cross section of H2S. *Chemical Physics Letters* 119(4):327-330.
41. Liu X*, et al.* (1999) Photodissociation of hydrogen sulfide at 157.6 nm: Observation of SH bimodal rotational distribution. *The Journal of Chemical Physics* 111(9):3940-3945.
42. Dixon RN, Marston CC, & Balint-Kurti GG (1990) Photodissociation dynamics and emission spectroscopy of H[sub 2]S in its first absorption band: A time dependent quantum mechanical study. *The Journal of Chemical Physics* 93(9):6520-6534.
43. Heumann B, Düren R, & Schinke R (1991) Ab initio calculation of the two lowest excited states of H2S relevant for the photodissociation in the first continuum. *Chemical Physics Letters* 180(6):583-588.
44. Muskatel BH, Remacle F, Thiemens MH, & Levine RD (2011) On the strong and selective isotope effect in the UV excitation of N2 with implications toward the nebula and Martian atmosphere. *Proceedings of the National Academy of Sciences* 108(15):6.
45. Chakraborty S, Davis RD, Ahmed M, Jackson TL, & Thiemens MH (2012) Oxygen isotope fractionation in the vacuum ultraviolet photodissociation of carbon monoxide: Wavelength, pressure, and temperature dependency. *The Journal of Chemical Physics* 137(2):024309-024312.
46. Bhattacharya SK, Savarino J, & Thiemens MH (2000) A new class of oxygen isotopic fractionation in photodissociation of carbon dioxide: Potential implications for atmospheres of Mars and Earth. *Geophysical Research Letters* 27(10):1459-1462.
47. Mahata S & Bhattacharya SK (2009) Anomalous enrichment of O-17 and C-13 in photodissociation products of CO2: Possible role of nuclear spin. (Translated from English) *Journal of Chemical Physics* 130(23) (in English).
48. Michalski G, Jost R, Sugny D, Joyeux M, & Thiemens M (2004) Dissociation energies of six NO[sub 2] isotopologues by laser induced fluorescence spectroscopy and zero point

energy of some triatomic molecules. *The Journal of Chemical Physics* 121(15):7153-7161.
49. Jost R, Michalski G, & Thiemens M (2005) Comparison of rovibronic density of asymmetric versus symmetric NO2 isotopologues at dissociation threshold: Broken symmetry effects. *Journal of Chemical Physics* 123(5).
50. Cliff SS, Brenninkmeijer CAM, & Thiemens MH (1999) First measurement of the O-18/O-16 and O-17/O-16 ratios in stratospheric nitrous oxide: A mass-independent anomaly. *Journal of Geophysical Research-Atmospheres* 104(D13):16171-16175.
51. Lyons JR (2007) Mass-independent fractionation of sulfur isotopes by isotope-selective photodissociation of SO2. *Geophys. Res. Lett.* 34(22):L22811.
52. Thiemens MH & Heidenreich JE (1983) The Mass-Independent Fractionation of Oxygen - A Novel Isotope Effect and Its Possible Cosmochemical Implications. *Science* 219(4588):1073-1075.
53. Gao YQ & Marcus RA (2001) Strange and Unconventional Isotope Effects in Ozone Formation. *Science* 293(5528):259-263.
54. Schmidt JA, Johnson MS, & Schinke R (2011) Isotope effects in N2O photolysis from first principles. *Atmos. Chem. Phys.* 11(17):8965-8975.
55. Cicerone RJ & McCrumb JL (1980) Photodissociation of isotopically heavy O 2 as a source of atmospheric O 3. *Geophys. Res. Lett.* 7(4):251-254.
56. Zahnle KJ & Walker JCG (1982) The evolution of solar ultraviolet luminosity. *Rev. Geophys.* 20(2):12.
57. Gail H-P (1998) Chemical reactions in protoplanetary accretion disks IV. Multicomponent dust mixture. *Astron. Astrophys.* 332:23.
58. Lauretta DS, Lodders K, & Fegley B (1997) Experimental Simulations of Sulfide Formation in the Solar Nebula. *Science* 277(5324):358-360.
59. Liffman K, Pignatale FC, Maddison S, & Brooks G (2012) Refractory Metal Nuggets -- Formation of the First Condensates in the Solar Nebula. *ArXiv e-prints*.
60. Russell SS, Srinivasan G, Huss GR, Wasserburg GJ, & MacPherson GJ (1996) Evidence for Widespread 26Al in the Solar Nebula and Constraints for Nebula Time Scales. *Science* 273(5276):757-762.
61. Itoh S & Yurimoto H (2003) Contemporaneous formation of chondrules and refractory inclusions in the early Solar System. *Nature* 423(6941):728-731.
62. Simon JI*, et al.* (2011) Oxygen Isotope Variations at the Margin of a CAI Records Circulation Within the Solar Nebula. *Science* 331(6021):1175-1178.
63. Stevenson DJ & Lunine JI (1988) Rapid formation of Jupiter by diffusive redistribution of water vapor in the solar nebula. *Icarus* 75(1):146-155.
64. Cyr KE, Sears WD, & Lunine JI (1998) Distribution and Evolution of Water Ice in the Solar Nebula: Implications for Solar System Body Formation. *Icarus* 135(2):537-548.
65. Ebel DS (2011) Sulfur in Extraterrestrial Bodies and the Deep Earth. *Reviews in Mineralogy and Geochemistry* 73(1):315-336.
66. Clayton RN & Mayeda TK (1988) Formation of ureilites by nebular processes. *Geochimica Et Cosmochimica Acta* 52(5):1313-1318.
67. Yang J & Epstein S (1983) Interstellar organic matter in meteorites. *Geochimica Et Cosmochimica Acta* 47(12):2199-2216.
68. Ciesla FJ & Sandford SA (2012) Organic Synthesis via Irradiation and Warming of Ice Grains in the Solar Nebula. *Science* 336(6080):452-454.

Figure Captions

Figure 1. Schematic diagram of the solar nebula showing the snowline which separates the inner and outer nebula.

Figure 2. (a) Sulfur isotopic fractionation ($\delta^{34}S$) and (b) the corresponding $\Delta^{33}S$ (mass independent component) values as observed in different group of meteorites. The achondrites show mass independent fractionation in bulk level. Only the chondrule rim (from Dhajala) show mass independent composition. All data taken from literature as mentioned in the text.

Figure 3. Three isotope diagrams showing the sulfur isotopic compositions measured in the present H_2S photolysis experiments. The left and right Y-axis represent $\delta^{33}S$ and $\delta^{36}S$, respectively. Mass dependent slope lines are shown for reference. The elemental sulfur samples for different VUV wavelengths yield mass independent sulfur isotopic composition. The circled data points are associated with larger uncertainties as describe in the text, otherwise, for all other data points the 1σ uncertainties are less than the size of the symbols.

Figure 4. $\Delta^{33}S$ vs. $\Delta^{36}S$ plot highlighting the mass independent fractionation measured during VUV photolysis of H_2S. The data from 121.6 nm (Lyman-α line) photolysis define a slope of ~ -3. The mean values of the meteorite data are plotted (6, 17), which showed a spread (though small) along the same line. The mass independent fractionation trends for other wavelengths are different than that of 121.6 nm as described in the text. The composition of organics from Murchison (16) are also shown and may be explained by some combination of fractionation by different wavelengths.

Figure 5. Solar luminosity at 1 My in VUV spectral region as reconstructed by (56). Lyman-α line at 121.6 nm is the strongest in the t-tauri phase of the sun. The wavelengths used in the present experiment are marked along with the integrated absorption cross-sections of H_2S (relative to the cross-section at 121.6 nm) in the parenthesis (34).

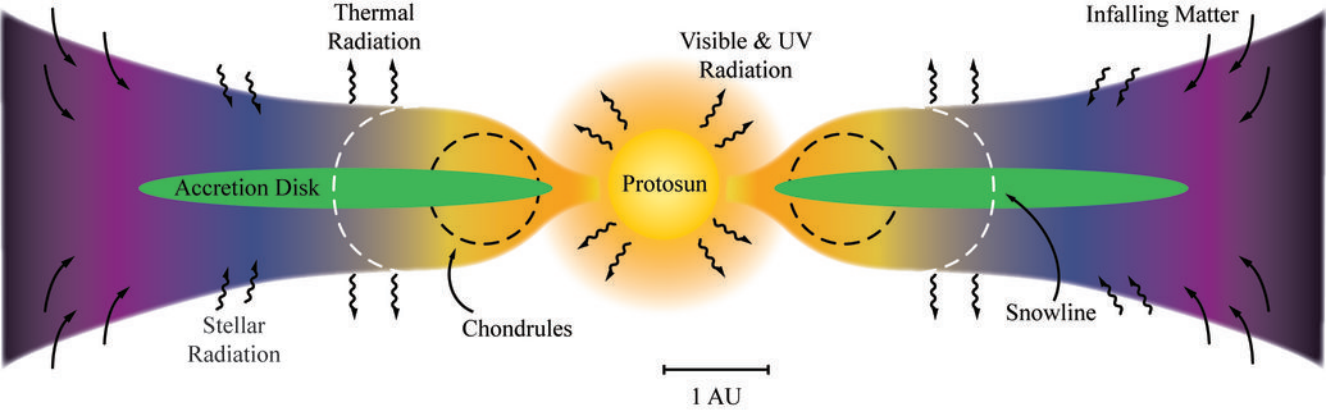
Thermal
Radiation
Visible & UV
Radiation
Infalling Matter
Accretion Disk
Protosun
Stellar
Radiation
Chondrules
Snowline
1 AU

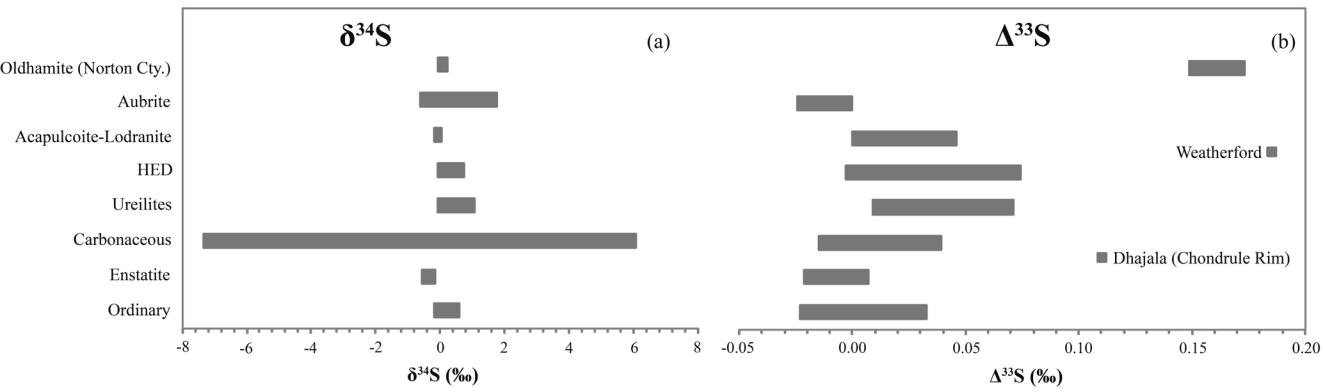
δ34S
(a)
Oldhamite (Norton Cty.)
Aubrite
Acapulcoite-Lodranite
HED
Ureilites
Carbonaceous
Enstatite
Ordinary
-8
-6
-4
-2
0
2
4
6
8
δ34S (‰)
Δ33S
(b)
Weatherford
Dhajala (Chondrule Rim)
-0.05
0.00
0.05
0.10
0.15
0.20
Δ33S (‰)

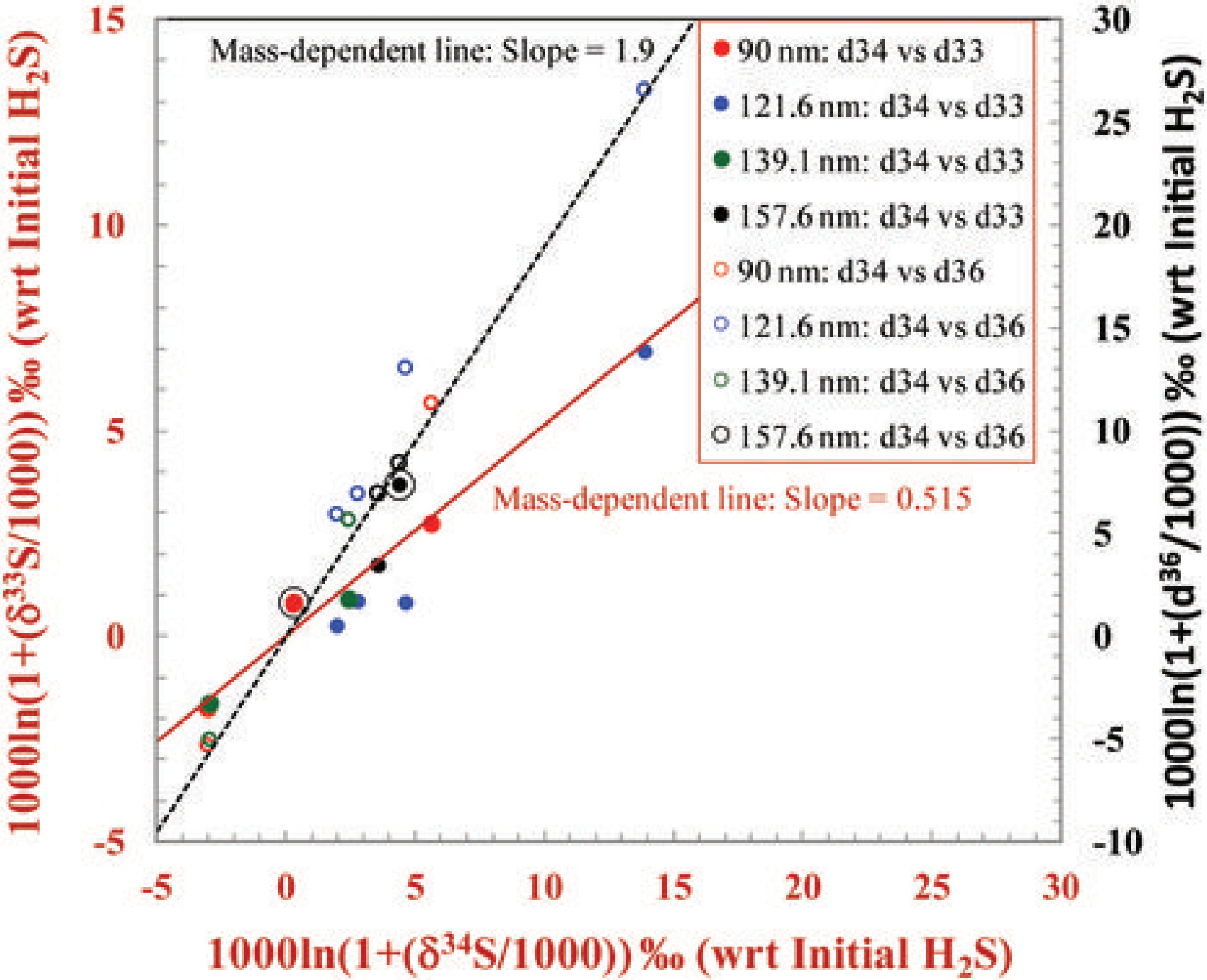
Mass-dependent line: Slope = 1.9
90 nm: d34 vs d33
121.6 nm: d34 vs d33
139.1 nm: d34 vs d33
157.6 nm: d34 vs d33
90 nm: d34 vs d36
121.6 nm: d34 vs d36
139.1 nm: d34 vs d36
157.6 nm: d34 vs d36
Mass-dependent line: Slope = 0.515
1000ln(1+(δ33S/1000)) ‰ (wrt Initial H2S)
1000ln(1+(δ34S/1000)) ‰ (wrt Initial H2S)
1000ln(1+(d36/1000)) ‰ (wrt Initial H2S)
15
10
5
0
-5
30
25
20
15
10
5
0
-5
-10
-5
0
5
10
15
20
25
30

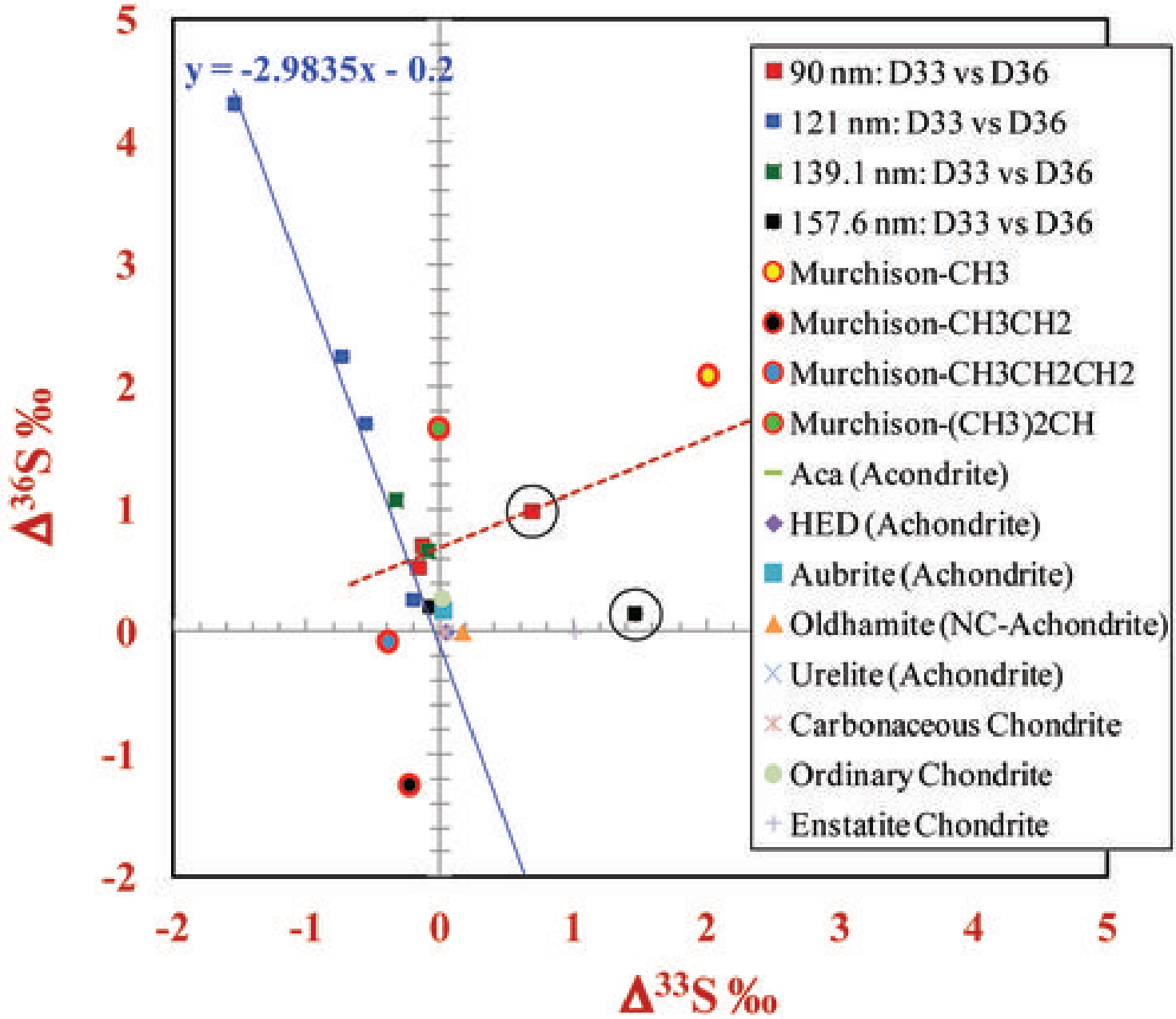
y = -2.9835x - 0.2
90 nm: D33 vs D36
121 nm: D33 vs D36
139.1 nm: D33 vs D36
157.6 nm: D33 vs D36
Murchison-CH3
Murchison-CH3CH2
Murchison-CH3CH2CH2
Murchison-(CH3)2CH
Aca (Acondrite)
HED (Achondrite)
Aubrite (Achondrite)
Oldhamite (NC-Achondrite)
Urelite (Achondrite)
Carbonaceous Chondrite
Ordinary Chondrite
Enstatite Chondrite
Δ36S ‰
Δ33S ‰
5
4
3
2
1
0
-1
-2
-2
-1
0
1
2
3
4
5

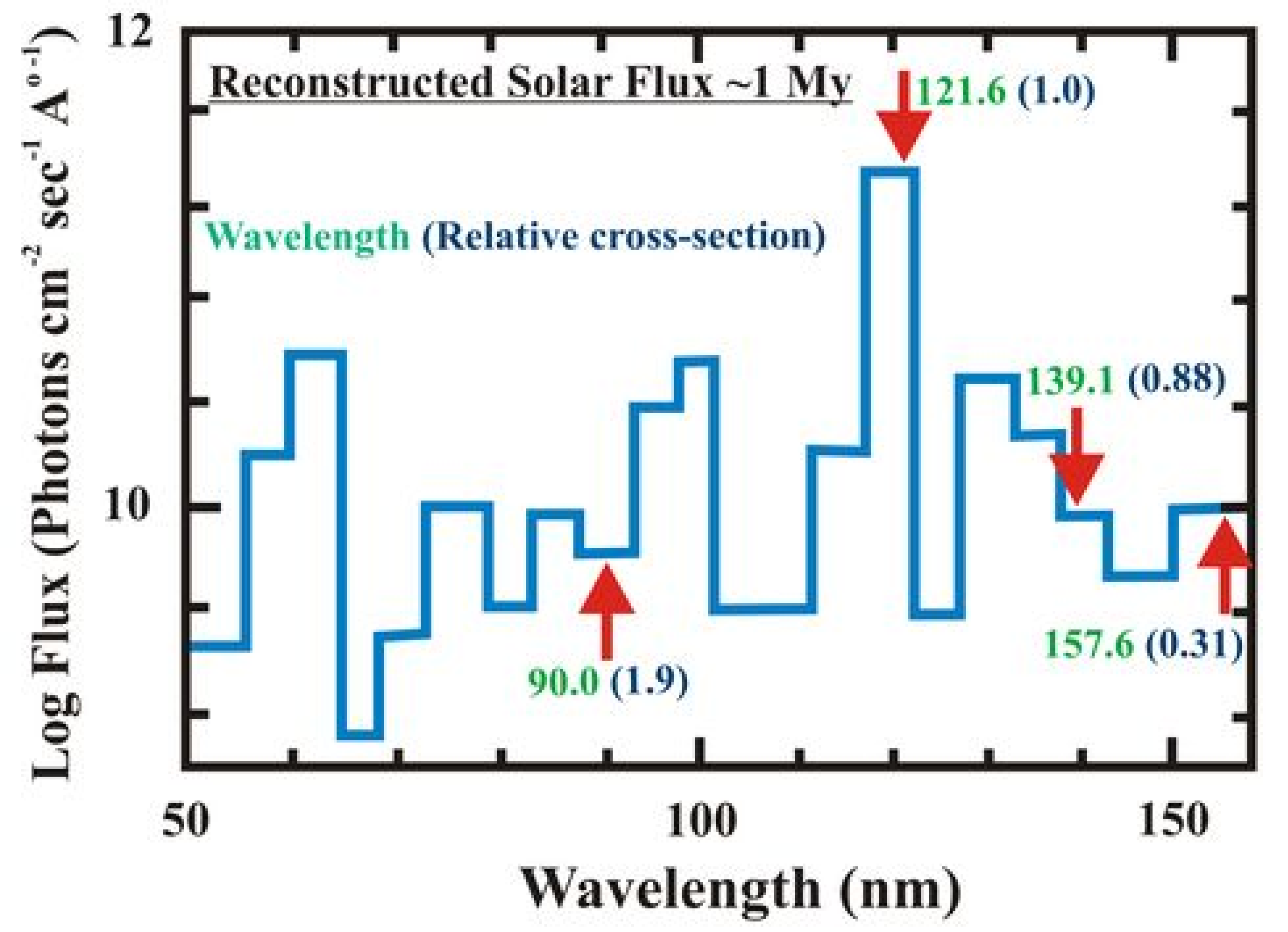
Reconstructed Solar Flux ~1 My
Wavelength (Relative cross-section)
121.6 (1.0)
139.1 (0.88)
157.6 (0.31)
90.0 (1.9)
Log Flux (Photons cm-2 sec-1 A0-1)
12
10
50
100
150
Wavelength (nm)